Atmospheric Research 169 (2016) 523–538

Contents lists available at ScienceDirect

Atmospheric Research

journal homepage: www.elsevier.com/locate/atmos

Numerical modeling of an intense precipitation event and its associated lightning activity over northern Greece

I. Pytharoulis *, S. Kotsopoulos, I. Tegoulias, S. Kartsios, D. Bampzelis, T. Karacostas

Department of Meteorology and Climatology, School of Geology, Aristotle University of Thessaloniki, Thessaloniki 54124, Greece

ARTICLE INFO

Article history:
Received 31 January 2015
Received in revised form 24 June 2015
Accepted 26 June 2015
Available online 2 July 2015

Keywords:
WRF numerical model
Intense precipitation
Neighborhood based verification
Lightning Potential Index
Topography
SRTM

ABSTRACT

This study investigates an intense precipitation event and its lightning activity that affected northern Greece and primarily Thessaloniki on 15 July 2014. The precipitation measurement of 98.5 mm in 15 h at the Aristotle University of Thessaloniki set a new absolute record maximum. The thermodynamic analysis indicated that the event took place in an environment that could support deep thunderstorm activity. The development of this intense event was associated with significant low-level convergence and upper-level divergence even before its triggering and a positive vertical gradient of relative vorticity advection. The high resolution (1.667 km × 1.667 km) non-hydrostatic WRF-ARW numerical weather prediction model was used to simulate this intense precipitation event, while the Lightning Potential Index was utilized to calculate the potential for lightning activity. Sensitivity experiments suggested that although the strong synoptic forcing assumed primary role in the occurrence of intense precipitation and lightning activity, their spatiotemporal variability was affected by topography. The application of the very fine resolution topography of NASA Shuttle Radar Topographic Mission improved the simulated precipitation and the calculated lightning potential.

1. Introduction

On 15 July 2014, Thessaloniki and Chalkidiki in northern Greece (Fig. 1) were affected by strong precipitation, which caused significant problems, including flood and damages to both infrastructure and cultivations in the city of Thessaloniki and the surrounding regions. The meteorological station of the Department of Meteorology and Climatology of the Aristotle University of Thessaloniki (AUTH), which is located near the city center, measured 98.5 mm of rain from 21:00 UTC on 14 July to 12:00 UTC on 15 July 2014. Almost all of the total rain amount (98.4 mm) was collected after 00:00 UTC, while the maximum rate reached 41.0 mm in 3 h. The station of the Hellenic National Meteorological Service (HNMS) at the airport of Thessaloniki (LGTS) recorded 61 mm of rain between 00:00 UTC and 12:00 UTC on 15 July. The measurement of AUTH is a record maximum, exceeding the previous absolute maximum of 98 mm (Anagnostopoulou and Tolika, 2012), which was observed in 24 November 1985. Similarly, the measurement of LGTS exceeded the maximum daily value of 60.2 mm, which appeared in the climatology of Kornaros (1999) for July 1959–1997. The fact that the mean annual precipitation is 449.6 mm at AUTH (Anagnostopoulou and Tolika, 2012) and 448.7 mm at LGTS (Kornaros, 1999) further exhibits the severity of the event.

Previous intense precipitation events that affected Greece have been investigated through both observational and/or modeling studies (e.g., Kallos and Pytharoulis, 2005; Kotroni et al., 1997, 1999; Lagouvardos et al., 1996; Papadopoulos, 2001). Such case studies offer a unique testbed for the investigation of the performance and tuning of modern numerical weather prediction models in extreme conditions. Kotroni et al. (1997) have shown that convergence zones promote summer storm activity in Greece, but, under weak synoptic flow. Lagouvardos et al. (1996) and Kotroni et al. (1999) have pointed out the role of orographic lifting in the eastern mainland of Greece in inducing heavy precipitation and floods.

Lightning activity was associated with the event of July 2014 and affected the entire region of Thermaikos Gulf and most of Chalkidiki. Lightning discharges are among the most impressive physical phenomena, but also highly lethal. They pose a serious threat to the physical environment because they are associated with wildfires, industrial accidents and power failures (Nie et al., 2008; Peterson et al., 2010; Renni et al., 2010), while they are equally dangerous to humans (Ashley and Gilson, 2009; Rakov and Uman, 2003). A football player died during training in Greece in November 2014, because of a cloud-to-ground lightning strike. Papagiannaki et al. (2013) reported 20 deaths due to lightning strikes in Greece from 2001 to 2011.

During the last years, the availability of modern lightning detection systems (e.g., ATD, LINET, WWLLN, ZEUS) has resulted to an increased interest in their study, prediction and use. A number of studies have recently appeared in the literature, investigating their statistical characteristics, their relationship with topography, terrain slope and vegetation in the Mediterranean basin and Greece (e.g., Defer et al., 2005; Katsanos et al., 2009; Kotroni and Lagouvardos, 2008; Mazarakis

* Corresponding author.
E-mail address: pyth@geo.auth.gr (I. Pytharoulis).

http://dx.doi.org/10.1016/j.atmosres.2015.06.019
0169-8095/

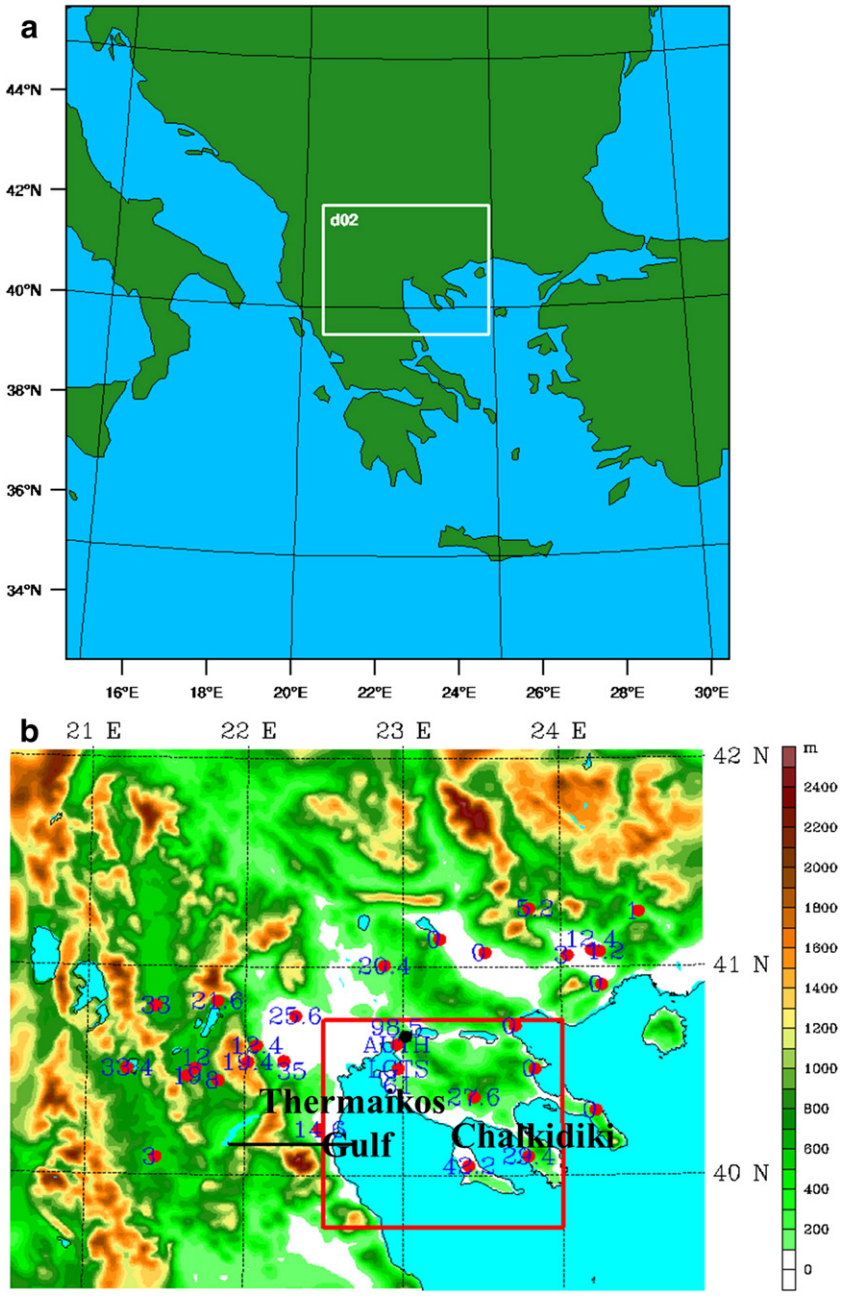

Fig. 1. (a) The two nests (D01, D02) used by WRF-ARW in the numerical experiments and (b) the topography of the inner domain and the locations of the available stations. In panel (b): i) the square indicates the region of interest (39.75°N–40.75°N, 22.5°E–24.0°E), ii) the numbers depict the observed 24 h accumulated precipitation (mm) from 18:00 UTC on 14 July to 18:00 UTC on 15 July 2014, iii) the black bullet indicates the location of the weather radar at Filyro, and iv) the black line depicts the area of the vertical section of Fig. 14.

et al., 2008; Nastos et al., 2014). Papadopoulos et al. (2005) developed a technique for the assimilation of lightning observations for a regional numerical weather prediction model, in order to improve the convective precipitation in the Mediterranean. Papadopoulos et al. (2009) successfully applied this methodology to represent the precipitation during a flood event. Fierro et al. (2012) assimilated total lightning data into the Weather Research and Forecasting (WRF) numerical model during the 24 May 2011 Oklahoma tornado outbreak and significantly improved the representation of convection at both the analysis and forecasts. More recently, Lynn et al. (2015) used the WRF model and the dynamic lightning model of Lynn et al. (2012), in four case studies with different convective regimes over the U.S.A., and showed that the assimilation of observed lightning improved the spatial distribution and intensity of forecast lightning.

A number of indices have been proposed in order to predict the lightning activity and not only the probability or severity of convection, based either on statistical methods or simplifications of the lightning physics (e.g., Bright et al., 2005; Dahl et al., 2011a,b; Lynn et al., 2012; Mazany et al., 2002; McGaul et al., 2009; Price and Rind, 1992; Yair et al., 2010). These indices may be calculated using radiosonde data, radar measurements or numerical weather predictions. The lack of lightning data prevented the use and validation of such techniques in Greece until recently (Giannaros et al., 2015; Pytharoulis et al., 2012; Yair et al., 2010).

The intense precipitation event of July 2014 and its associated lightning activity offered the motivation and the chance to test the performance of the state-of-the-art WRF numerical weather prediction model along with the Lightning Potential Index (LPI) of Yair et al.

(2010). The first two aims of this study are: a) the examination of the synoptic/mesoscale conditions that influenced this severe rain and lightning event's development and b) the investigation of the forecast accuracy of the WRF model at extremely high resolution with explicit microphysics and the LPI to realistically predict precipitation and the potential for lightning activity. Moreover, this incident took place in a region with varying physiographic characteristics and complex terrain. Although, several studies (e.g., Kotroni et al., 1999; Lagouvardos et al., 1996) have pointed out the role of orography of the eastern mainland of Greece in inducing heavy precipitation, Matsangouras et al. (2014) suggested that topography may not always have a strong influence on high impact weather events that develop under strong synoptic forcing, even in cases of significant topographical variation. Therefore, the third aim of this study is the investigation of the role of topography in the development of the July 2014 event.

The following section describes the utilized data and the setup of the numerical model. The synoptic and mesoscale analysis is performed in Section 3, while Section 4 analyzes the numerical experiments. Finally, conclusions are drawn in the last section.

2. Data and numerical model setup

In this study, surface and upper air measurements, lightning observations and gridded analyses were utilized along with the Weather Research and Forecasting numerical weather prediction model. The surface observations (Fig. 1b) were retrieved by the automatic weather stations of the National Observatory of Athens (NOA) at 27 locations in northern Greece, the meteorological station of AUTH, which is located in the city of Thessaloniki, and the station of HNMS at the airport of Thessaloniki (LGTS; about 12–13 km south of AUTH). The radiosonde observations were also derived from the latter station. The lightning data were provided by the ground-based ZEUS network operated by NOA. ZEUS is a very low frequency (VLF) based lightning detection system. It is capable to detect not only cloud-to-ground, but also intra-cloud lightning discharges (Lagouvardos et al., 2009; Yair et al., 2010). However, Lagouvardos et al. (2009) showed that ZEUS has a reduced efficiency to detect intra-cloud strokes compared to cloud-to-ground ones. Detailed presentation of the system is given in Kotroni and Lagouvardos (2008) and Lagouvardos et al. (2009).

Precipitation data were also available from the C-band weather radar of 3D S.A. company (http://www.3dsa.gr), which is located at Filyro (40.672°N, 23.014°E) northeast of Thessaloniki (Fig. 1b). The data were disseminated and used up to a radius of 100 km because of the existence of high topography at larger distances. This radar is operationally used by the Greek Agricultural Insurance Organization in the hail suppression program which runs from spring to autumn each year since 1984 (Karacostas, 1984). The precipitation estimation was based on radar reflectivity measurements using the Marshall–Palmer relationship with constant values a = 200 and b = 1.3. These constants were derived after calibration that took place by the Meteorological Applications Department of the Greek Agricultural Insurance Organization (Sioutas and Rudolph, 1993), to fit summertime convective rainfall in Northern and Central Greece. The precipitation amounts were interpolated from the radar grid (750 m × 750 m) to the mesh of WRF-D02 through the Climate Data Operators (CDO) software using the first order conservative remapping that conserves the total amount of rain which has fallen in an area.

The observations were combined with gridded surface and upper-air analyses of the European Centre for Medium-Range Weather Forecasts (ECMWF). The analyses were retrieved near and at the surface and on isobaric surfaces at 6-hourly intervals on a regular 0.125° lat. × 0.125° lon. grid.

The nonhydrostatic Weather Research and Forecasting model with the Advanced Research dynamic solver (Version 3.5.1) was utilized in the numerical experiments (Skamarock et al., 2008; Wang et al., 2013). Two interactive model domains covered the wider area of the Balkan peninsula (D01; Fig. 1a) and northern Greece (D02; Fig. 1b) at horizontal grid-spacing of 5 km and 1.667 km, respectively. The inner domain was two-way nested to its parent one. Following Mass et al. (2002), a very fine resolution was employed in D02, in order to provide a more accurate representation of the meteorological conditions in the area of interest, which is characterized by significant variability of the physiographic characteristics and terrain. The operational analyses of the European Centre for Medium Range Weather Forecasts at 6-hourly intervals (0.125° × 0.125° lat.–long.) were used as initial and boundary conditions of the coarse domain in the numerical experiments. The sea-surface temperatures were provided by the National Centers for Environmental Prediction (NCEP) at a fine horizontal grid increment of 1/12° × 1/12° lat.–long. (~0.083° × 0.083°), and remained fixed to the initial values throughout the forecast horizon. In the vertical, both nests employed 51 sigma levels (up to 50 hPa) with increased resolution in the boundary layer.

Fine resolution data were used for the definition of topography at both nests. The topography of the control run was derived from the United States Geological Survey (USGS) at a resolution of 30 arc sec × 30 arc sec lat.–long. The very fine resolution dataset (3 arc sec × 3 arc sec lat.–long.) of NASA Shuttle Radar Topographic Mission (SRTM) was employed in the second numerical experiment. These data were retrieved from the Consortium for Spatial Information (CGIAR-CSI) of the Consultative Group for International Agricultural Research (CGIAR), which has subjected the original SRTM data to a number of processing steps to create and offer a post-processed 3 arc sec × 3 arc sec (latitude–longitude) topography dataset for the globe (http://srtm.csi.cgiar.org).

The RRTMG (rapid radiative transfer model application for global climate models) (Iacono et al., 2008), the Monin–Obukhov (MM5) and the Yonsei University (YSU; Hong et al., 2006) schemes were used in all nests to represent longwave/shortwave radiation, surface layer, and boundary layer processes, respectively. The YSU scheme and its preceding version of Hong and Pan (1996) have been used for precipitation forecasting over the complex terrain of Greece (e.g., Mazarakis et al., 2009; Bartzokas et al., 2010; Efstathiou et al., 2013; Sindosi et al., 2015) and worldwide (e.g., Hong et al., 2006). Efstathiou et al. (2013) examined the sensitivity of the WRF model rainfall predictions to the choice of boundary layer schemes, through the simulation of an exceptionally heavy rainfall event over Chalkidiki in northern Greece. They showed that configurations using YSU scheme provided better statistical scores for heavy precipitation than the ones with Mellor–Yamada–Janjic boundary layer scheme. The soil processes were represented by the NOAH (NCEP/Oregon State University/Air Force/Hydrologic Research Lab) Unified model (Chen and Dudhia, 2001) in four layers (0–10, 10–40, 40–100, and 100–200 cm). Cumulus convection was parameterized only in the outer nest (D01) by the most recent version of the Kain–Fritsch scheme (Kain, 2004). The WRF Single-Moment 6-class scheme (WSM6; Hong and Lim, 2006), which includes separate variables for cloud water, rain, ice, snow and graupel, was employed at both nests in order to parameterize the microphysical processes. This scheme is suitable for the calculation of the lightning potential because it calculates the masses of liquid water, ice, snow and graupel.

Each numerical experiment had a horizon of 30 h and was initialised at 12:00 UTC on 14 July 2014 (i.e., about half a day before the onset of the event). The initialization time was selected in order to allow enough time for the model spin up. The model outputs were retrieved at 5 min intervals, so as to provide sufficient time resolution for the detection of the convective storms and the estimation of lightning potential and strikes.

3. Synoptic and mesoscale analysis

3.1. Description of the event

The lightning activity during the first half of 15 July 2014 in Thermaikos Gulf, Thessaloniki and Chalkidiki was characterized by two bursts. The first convective storms with lightning developed over

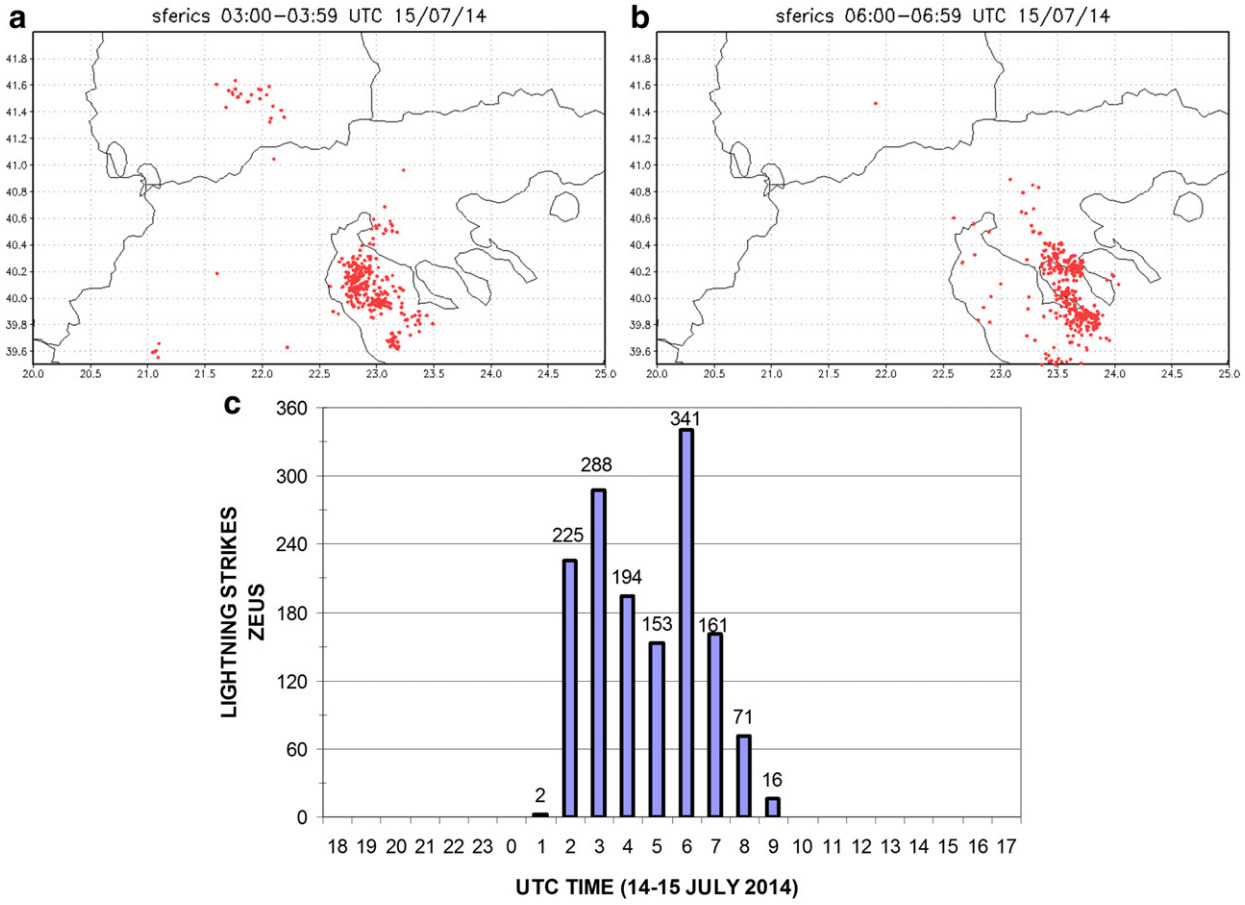

Fig. 2. a, b) The locations of the observed lightning strikes from 03:00 UTC to 03:59 UTC and from 06:00 UTC to 06:59 UTC on 15 July 2014, and (c) the timeseries of the hourly number of the observed lightning strikes in the area between 39.75°N–40.75°N and 22.5°E–24.0°E (Zeus data). In panel (c), the number of lightning at each hour T corresponds to the period from T:00 to T:59 UTC time.

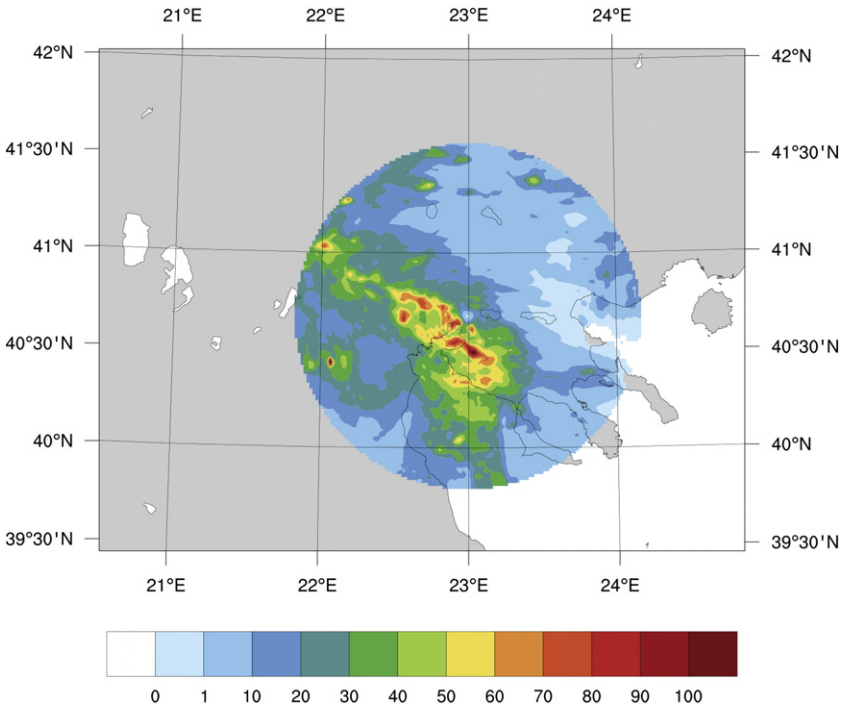

Fig. 3. 24-hour accumulated precipitation (18:00 UTC 14 July to 18:00 UTC 15 July 2014) estimated from the weather radar at Filyro. The color scale indicates the precipitation amount in mm. The location of the radar is depicted in Fig. 1b.

the land northwest of the city of Thessaloniki and in the Gulf of Thermaikos between 01:00 and 02:00 UTC. Two hours later (between 03:00–03:59 UTC), thunderstorms affected the entire area of Thessaloniki and the Thermaikos Gulf (Fig. 2a) and the total number of strikes rose to 288 (Fig. 2c) in the area of interest (39.75°N–40.75°N, 22.5°E–24.0°E). In the following hours, the main center of lightning activity moved over Chalkidiki, while it continued to affect the wider area of Thessaloniki (Fig. 2b). The maximum hourly number of strikes (341) was observed between 06:00 and 07:00 UTC in this region. Their total number during the event (01:00–09:59 UTC) was equal to 1451, which corresponds to a density of 1 strike per 10 km^2.

The locations of Thessaloniki, Chalkidiki and the Gulf of Thermaikos were affected by intense precipitation and lightning. Thus, in this study, the area of interest was considered to extend from 39.75°N to 40.75°N and from 22.5°E to 24.0°E (Fig. 1b). Small changes to its size would affect the total number of strikes, but not the conclusions about the evolution of the event. Moreover, the use of a much larger or smaller area was avoided, because in the former case the lightning of the surrounding regions would be erroneously considered, while in the latter case the actual activity would not be represented adequately due to its spatial extent (Fig. 2) and possible location errors by Zeus system (~6.8 km; Lagouvardos et al., 2009).

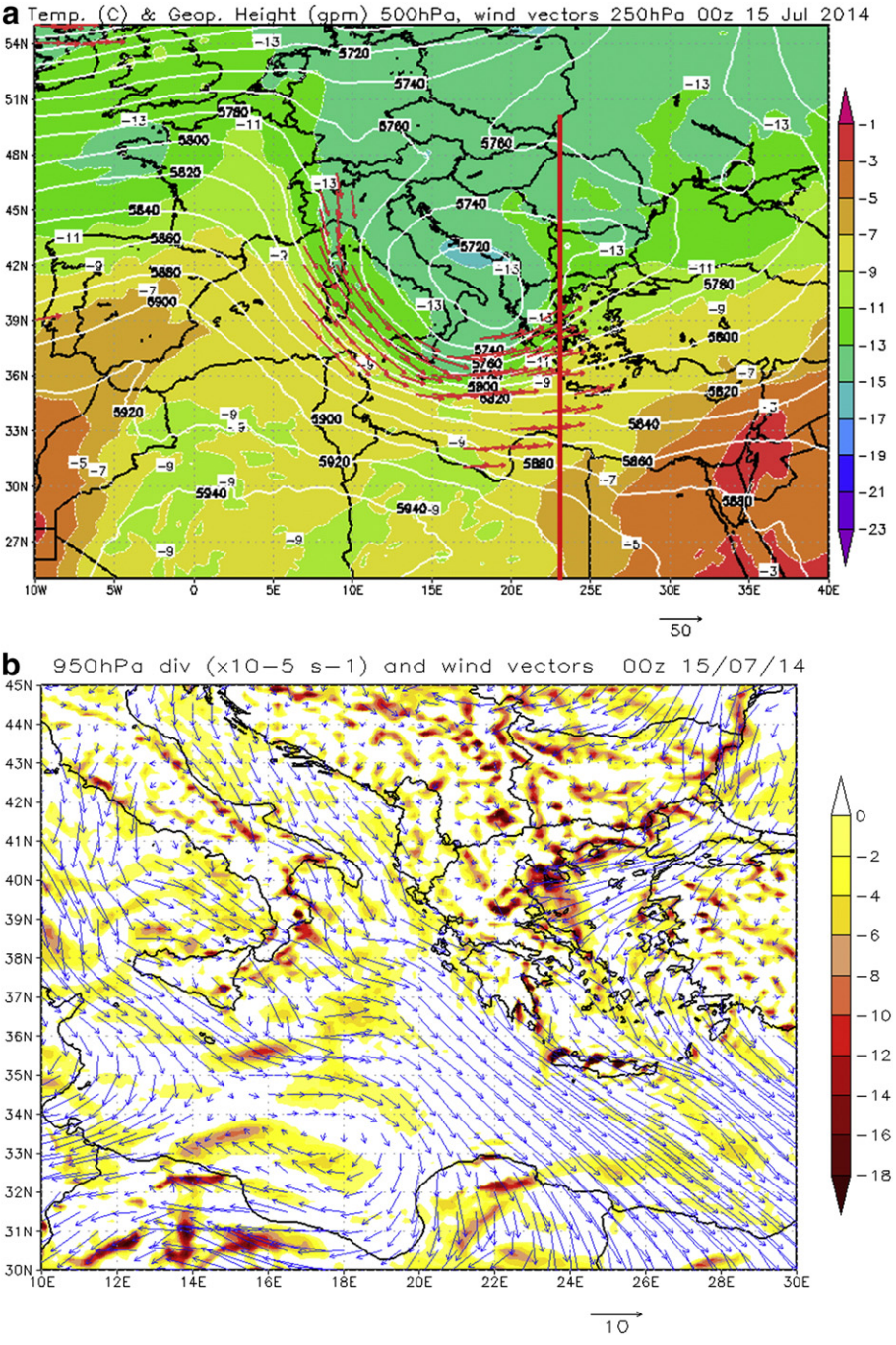

Fig. 4. a) Temperature (°C; shading), geopotential height (gpm; contours) at 500 hPa and wind vectors (>30 m/s; in red color) at 250 hPa, and b) divergence ($\times 10^{-5}$ s^{-1}; shading) and wind vectors at 950 hPa, at 00 UTC, 15 July 2014. In panel (a), the thick red line at 23°E indicates the location of the vertical section of Fig. 5. The vectors below each panel correspond to the reference wind speed of 50 m/s and 10 m/s (ECMWF analyses).

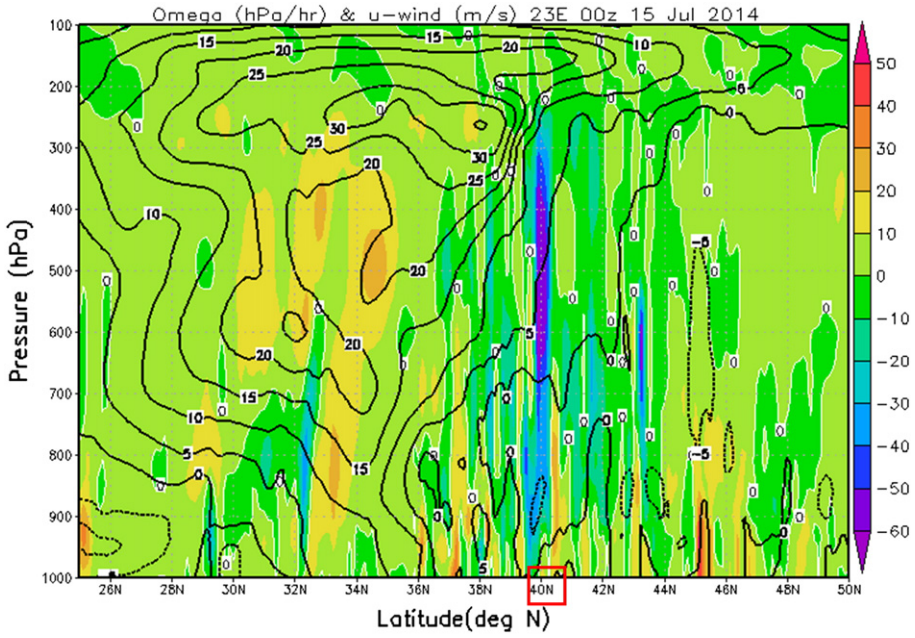

Fig. 5. Latitude–pressure section of u-wind component (m/s; contours) and omega (hPa/h; shading) at 23°E at 00 UTC, 15 July 2014. The region of this section is depicted in Fig. 4a. The red rectangle below the figure indicates the area of interest (ECMWF analyses).

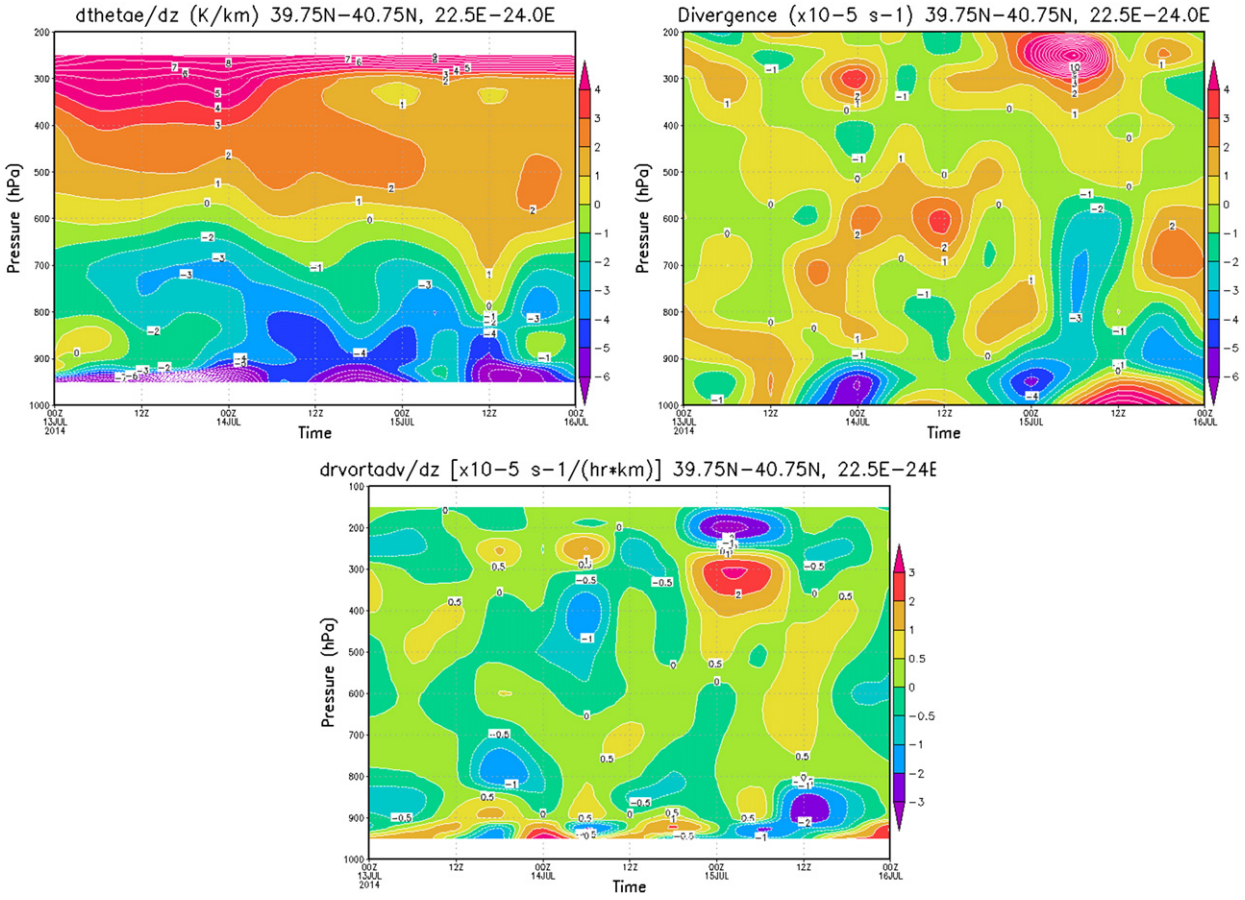

Fig. 6. Hovmoller diagrams of the vertical gradient of equivalent potential temperature (K/km), divergence ($\times 10^{-5}$ s^{-1}) and vertical gradient of relative vorticity advection ($\times 10^{-5}$ s^{-1} h^{-1} km^{-1}) averaged in the square shown in Fig. 1b (39.75°N–40.75°N, 22.5°E–24.0°E) (ECMWF analyses).

Table 1
The Mean Error (ME; model − observation), Mean Absolute Error (MAE) and Root Mean Square Error (RMSE) of the WRF-D02 simulated mean sea-level pressure (mslp), 2 m temperature (T2m), 2 m relative humidity (RH2m) and 2 m dew point temperature (Td2m) at the locations of the 27 NOA stations and LGTS from 18:00 UTC on 14 July (T + 6 h) to 18:00 UTC on 15 July 2014 (T + 30 h) in the control simulation (experiment 1). The interpolation method of distance weighted mean (from the values of the 4 surrounding gridpoints) was utilized to derive the forecast values at the location of each station. The values in brackets indicate the lower and upper limits of the confidence interval at the 95% significance level.

Parameter	ME	MAE	RMSE
mslp (hPa)	0.5 (0.37, 0.63)	1.4 (1.31, 1.49)	1.8 (1.74, 1.94)
T2m (K)	1.0 (0.81, 1.13)	1.8 (1.71, 1.93)	2.3 (2.19, 2.44)
RH2m (%)	−9.0 (−9.93, −8.07)	12.3 (11.65, 12.98)	15.4 (14.66, 16.17)
Td2m (K)	−1.3 (−1.45, −1.20)	1.8 (1.72, 1.90)	2.2 (2.13, 2.35)

The precipitation exhibited a significant spatial variability in northern Greece (Figs. 1b, 3). This is frequently observed in convective events. The station of the Department of Meteorology and Climatology of AUTH (very close to the town center) recorded the maximum value of 98.5 mm, from 18:00 UTC on 14 July to 18:00 UTC on 15 July 2014. The maximum rate reached 41 mm/3 h in each one of the periods 00:00–03:00 UTC and 06:00–09:00 UTC on 15 July 2014. These high intensities, as well as the extreme total amount of precipitation, were responsible for the floods in Thessaloniki. Regarding other locations in the area of interest, large amounts were also observed at the airport of Thessaloniki — LGTS (61.0 mm) and at Kassandria (42.2 mm), Marmaras (29.4 mm) and Polygyros (27.6 mm) in western and central Chalkidiki. Amounts of 98.4 mm at AUTH and 61.0 mm at LGTS were measured between 00:00 and 12:00 UTC on 15 July. Fig. 1b shows that large amounts, in excess of about 25 mm, were also measured north and northwest of the area of interest in the same period (e.g., 35 mm at Veroia, which is located about 62 km west of AUTH). In agreement with the station observations, the radar estimated precipitation showed intense precipitation above 30–40 mm in large regions of Thessaloniki, Thermaikos Gulf and western Chalkidiki (Fig. 3). More locally, in the areas near the city and the airport of Thessaloniki daily precipitation amounts of 60 mm or above were calculated. It is noted that the station measurements of 42.2 mm and 29.4 mm at the western and central peninsula of Chalkidiki (Fig. 1b) are not in agreement with the radar data. Therefore, the radar derived precipitation was not used: i) over and between the western and central peninsula of Chalkidiki (Kassandra and Sithonia, respectively) southeast of the radar, due to the mountains located in this direction, and ii) in the cone of silence.

3.2. Synoptic analysis

Over the two days prior to the precipitation/lightning event of this study, the synoptic situation in the central and eastern Mediterranean Sea was dominated by the passage of two mid-tropospheric troughs, with the second one being responsible for the severe weather. At 500 hPa, the second trough appeared between France and Italy at 00 UTC on 14 July 2014 and in the following hours it moved southeastward along Italy while it was transformed into a closed low. The system was located over the southern Adriatic Sea and the northern Ionian Sea at 00 UTC on 15 July (Fig. 4a), just before the onset of the lightning activity in the area of interest and the intense precipitation in Thessaloniki. Afterwards, the center of the closed low moved over central and northern Greece and colder air masses (of about −13 °C) were advected at 500 hPa over the area of interest.

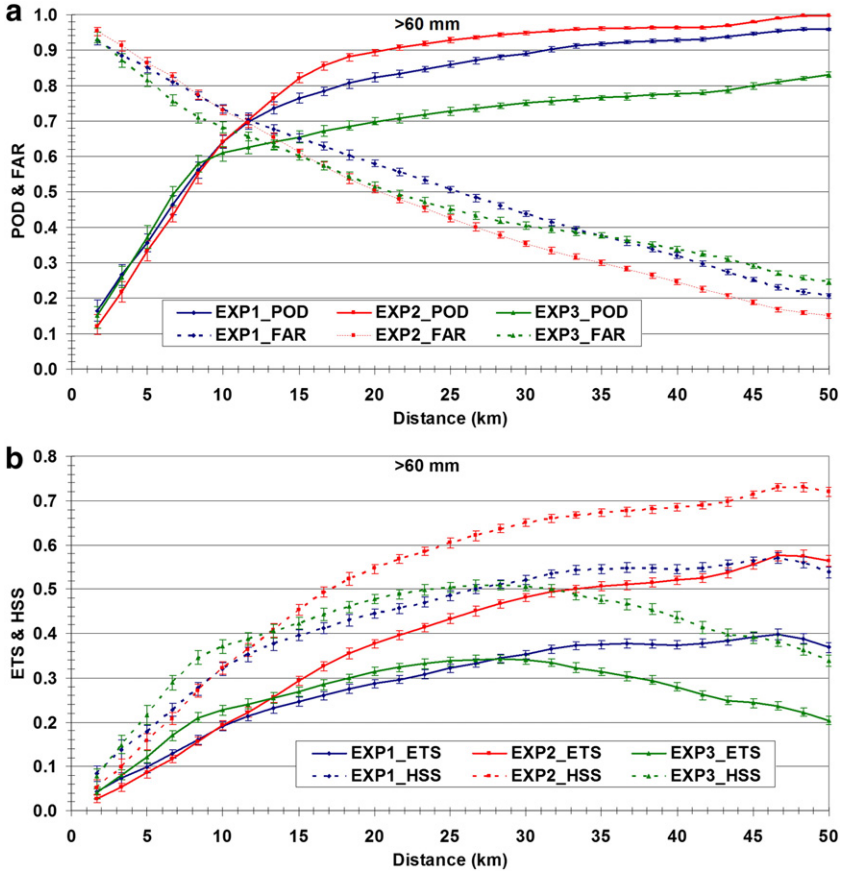

Fig. 7. a) Probability of Detection (POD) and False Alarm Ratio (FAR), and b) Equitable Threat Score (ETS) and Heidke Skill Score (HSS), of the 24 h simulated accumulated precipitation (WRF-D02) from 18:00 UTC on 14 July (T + 6 h) to 18:00 UTC on 15 July 2014 (T + 30 h) in the three experiments for different Distances (km) at the threshold of 60 mm. The confidence intervals at the 95% significance level are also plotted.

In the upper troposphere, the jet-stream was located above the mid-tropospheric baroclinic zone south of the closed low at 00 UTC on 15 July (Fig. 4a). At that time, the area of interest was located at the left flank of the jet-stream exit and its divergence reached about $15 \cdot 10^{-5}$ s^{-1} at 250 hPa. The indirect secondary circulation that arises at the exit of the jet streams is associated with upwards motions and upper level divergence at its left flank. Fig. 5 shows that upward velocities, up to about −50 to −60 hPa/h, occurred throughout the troposphere over the area of interest at 00 UTC on 15 July.

At mean sea-level, the combination of the stationary low pressure system of the Anatolian plateau with the higher pressures to the west resulted to an almost north–south orientation of the isobars over the Aegean sea (not shown). The low-level wind pattern resembled the Etesian winds with easterly–northeasterly, northerly and northwesterly flow over northern, central and southern Aegean sea (Fig. 4b), respectively. Fig. 4b also shows strong low-level convergence zones (up to about $-18 \cdot 10^{-5}$ s^{-1} at 950 hPa) over the Thermaikos Gulf and Chalkidiki at 00 UTC on 15 July, induced by the abovementioned synoptic flow. Kotroni et al. (1997) have shown that convergence zones promote summer storm activity in Greece, but, under weak synoptic flow.

3.3. Thermodynamic structure of the troposphere

The radiosonde ascent at the airport of Thessaloniki, which took place at 00 UTC on 15 July 2014 (not shown), exhibited the existence of conditional instability from the surface up to 600 hPa, while the temperature followed the moist adiabat above that level. The convective available potential energy (CAPE) exhibited a large value (1386 J/kg) and the convective inhibition (CIN) was −61.5 J/kg. The University of Wyoming provided access to the radiosonde data and calculated the thermodynamic variables. Therefore, the thermodynamic structure of the atmosphere was favorable for strong and deep convection (up to about 233 hPa). However, a mechanism was necessary in order to surpass the negative energy region and lift the air mass up to the level of free convection.

The widely used instability indices K and LI (lifted index), which were calculated by the University of Wyoming using the above radiosonde ascent, provided a good indication of the intensity of the convective activity prior to its triggering. K index was equal to 34.1, suggesting 85% probability of thunderstorm occurrence (following Yair et al., 2010). The LI (−3.84) indicates that thunderstorms are probable, but not likely to be severe. It needs to be noted that the values of both K and LI indices were close to the threshold of the next category which suggests “100% chance for thunderstorms” and “severe thunderstorms are possible”, respectively.

3.4. Time evolution of dynamic and thermodynamic parameters

The time evolution of the area averaged values of the vertical gradient of the equivalent potential temperature, the divergence and the vertical gradient of the advection of relative vorticity in the area of interest (39.75°N–40.75°N, 22.5°E–24.0°E) are presented in Fig. 6. They were estimated from the gridded ECMWF analyses using second order centered finite differences for the calculation of the horizontal and vertical gradients. The vertical gradient of the equivalent potential temperature showed a prolonged period of instability (Fig. 6 top left panel). The maximum value of the gradient reached about −8 to −9 K at low levels a few hours before the event. A lifting mechanism was needed in order to raise the potentially unstable layer to saturation and trigger the instability. Fig. 6 top right and bottom panels show that the prevailing synoptic conditions played a significant role in providing this mechanism. Both the low-level convergence and the upper-level divergence started to increase at the late hours of 14 July (i.e., a few hours before the triggering of the convective activity), and allowed the lifting of the air masses, and contributed to the development of strong vertical motions. Moreover, upward motions would be expected to be associated with the positive values of the vertical gradient of relative vorticity advection, observed in almost the whole troposphere after 00 UTC on 15 July, ahead of the approaching closed mid and upper-tropospheric low (Holton, 1992). It is noted that the potential vorticity anomaly associated with the closed low would also be expected to modulate the static stability below it (Hoskins et al., 1985), enhancing the probability of convection.

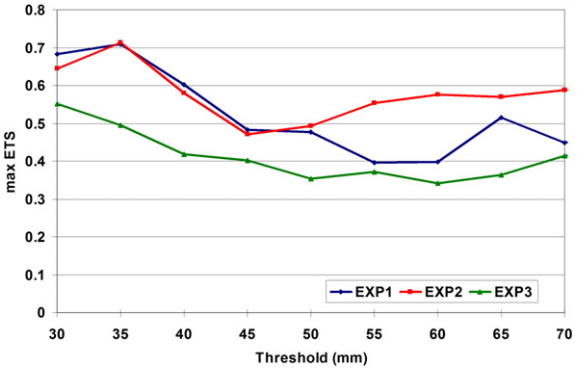

Fig. 8. The maximum ETS values of the 24 h precipitation forecasts (18:00 UTC 14 July to 18:00 UTC 15 July 2014) for different thresholds in the three experiments. At each threshold, the maximum ETS at Distances from 0 to 50 km (i.e., for neighborhood regions up to 100 km × 100 km) is plotted.

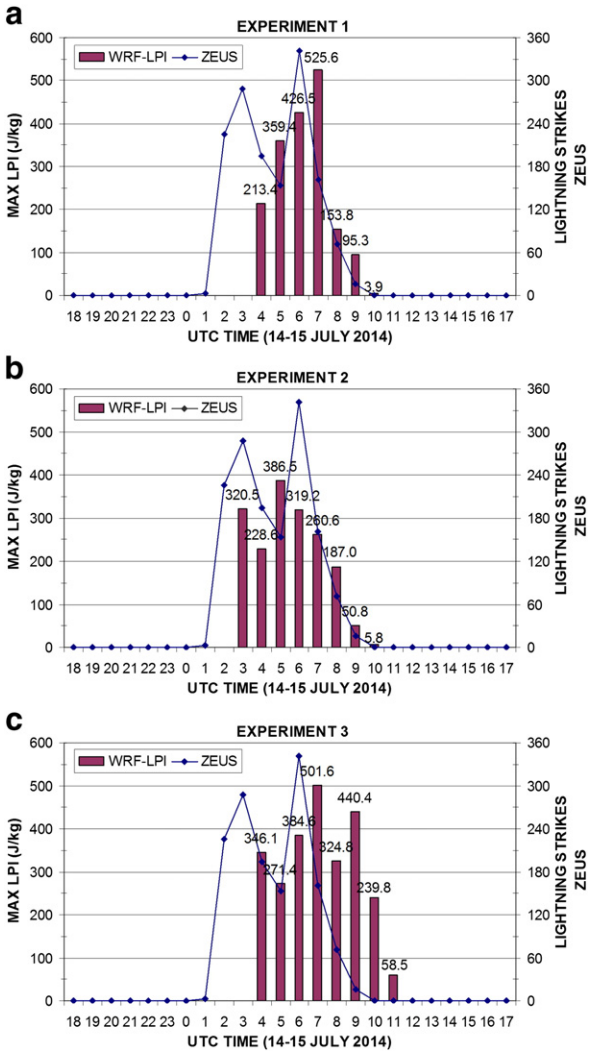

Fig. 9. Timeseries of WRF-D02 simulated maximum LPI (J/kg) and the number of observed lightning strikes (by Zeus system) between 39.75°N–40.75°N and 22.5°E–24.0°E.

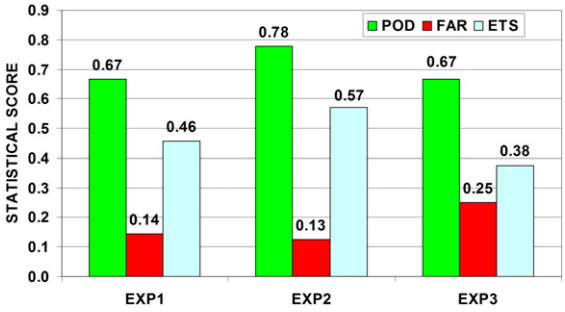

Fig. 10. Probability of Detection (POD), False Alarm Ratio (FAR) and Equitable Threat Score (ETS) of the WRF-D02 simulated maximum hourly LPI between 39.75°N–40.75°N and 22.5°E–24.0°E from 18:00 UTC on 14 July to 18:00 UTC on 15 July 2014 in the three experiments.

4. Numerical experiments

The intense precipitation event of 15 July 2014 and its associated lightning episodes were simulated using the WRF model. The lightning activity was represented through the Lightning Potential Index. According to Yair et al. (2010) who introduced this index, "in a developing thunderstorm, the LPI is the kinetic energy of the updrafts, scaled by the potential for charge separation within the main charging zone of the cloud (0 °C to −20 °C)". LPI does not calculate the electric charge, but the potential of the thundercloud to separate the charge in the cloud layer between 0 °C and −20 °C. It is estimated through the model predicted values of vertical velocity, liquid water, cloud ice, snow and graupel (Yair et al., 2010).

4.1. Model verification

The verification of the control simulation (experiment 1, hereafter) was performed using first all the available surface observations in D02 and the radiosonde data of the airport of Thessaloniki against the WRF-D02 values. Results during the first 6 h of simulation (during "spin-up") were ignored. Therefore, the model was verified from 18:00 UTC on 14 July to 18:00 UTC on 15 July 2014. The interpolation method referred to as "Distance Weighted Mean" (from the values of the 4 surrounding gridpoints) was used to derive the simulated values at the location of each station. According to the manual of the Model Evaluation Tool (MET) of WRF which was used for the verification, the weight given to each gridpoint is the reciprocal of the square of the distance from the actual location of each station. The weighted sum of simulated values is normalized by dividing by the sum of the weights. The pairs of observed versus model simulated values were created using mean sea-level pressure (mslp), 2 m air temperature (T2m), 2 m air relative humidity (RH2m) and 2 m dew point temperature (Td2m) measurements from 28 stations. These were the 27 automatic NOA stations in hourly intervals and LGTS in 3-hourly intervals (SYNOP reports).

The errors of simulated mslp, T2m, RH2m and Td2m in WRF-D02 and their confidence intervals at the 95% significance level (using the bootstrapping statistical method) are illustrated in Table 1. The model overestimated mslp and T2m by 0.5 hPa and 1.0 K, while it underestimated RH2m and Td2m by 9.0% and 1.3 K, respectively. The MAE (and RMSE) of mslp, T2m, RH2m and Td2m were 1.4 hPa (1.8 hPa), 1.8 K (2.3 K), 12.3% (15.4%) and 1.8 K (2.2 K), respectively. These scores are in general agreement with the ones that appear in the literature for modern high resolution numerical weather prediction

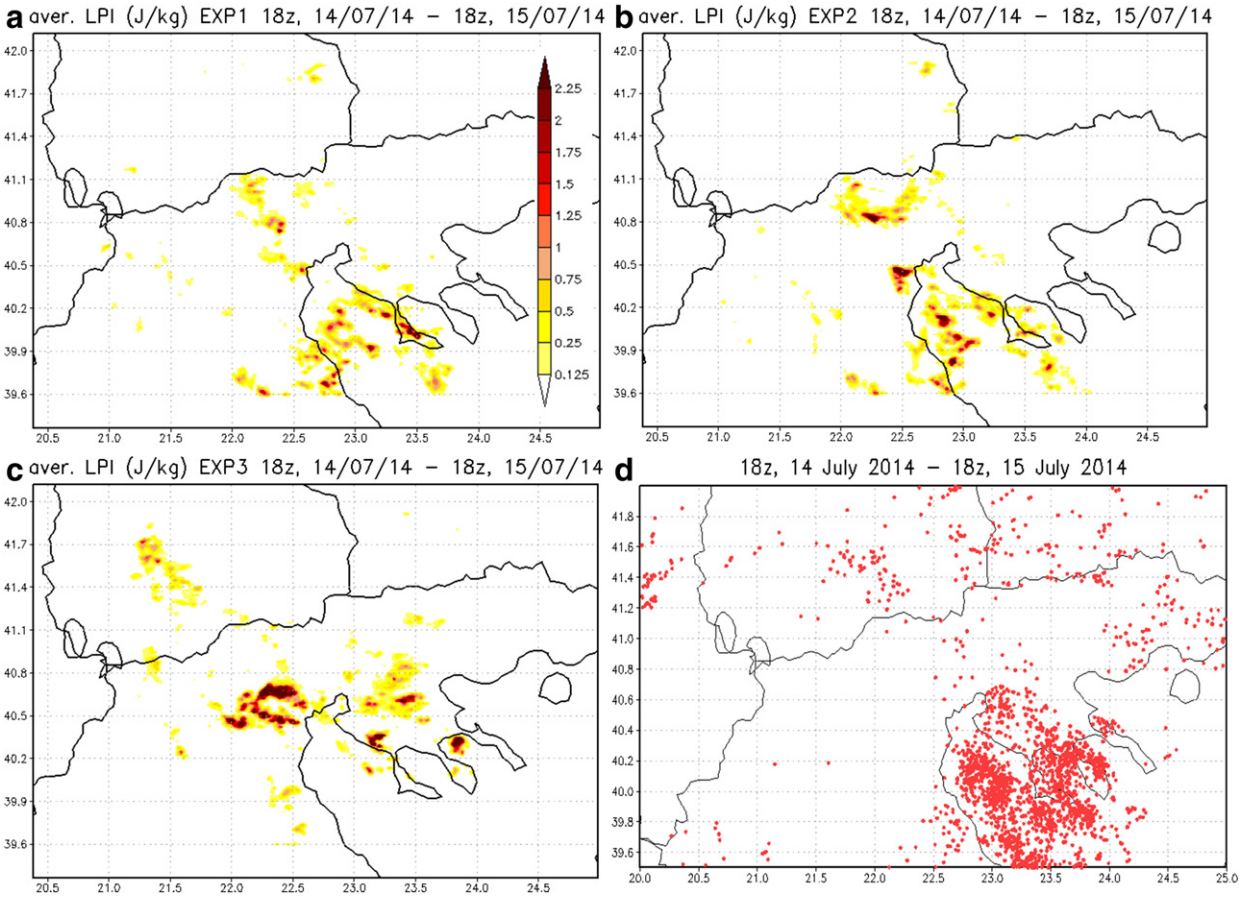

Fig. 11. a, b, c) The average value of LPI (J/kg) in the three experiments, and d) the locations of lightning strikes detected by Zeus system, from 18:00 UTC on 14 July to 18:00 UTC on 15 July 2014. The color scale indicates the average LPI in J/kg.

models in Greece and eastern Mediterranean. Papadopoulos and Katsafados (2009) evaluated the POSEIDON forecasting system (0.05° × 0.05°) across the eastern Mediterranean from mid-November 2007 to October 2008 and obtained RMSE between 1.2 and 1.8 hPa for mslp and 2.3 to 2.9 K for T2m, in the first 2 forecast days. Pytharoulis et al. (2014) validated the operational WRF-ARW modeling system of the Department of Meteorology and Climatology of AUTH at a resolution of 5 km × 5 km. They calculated the model errors over the wider Greek area in 2013. The MAEs of mslp, T2m and RH2m were about 1.1 to 1.8 hPa, 1.8 to 2.1 K and 11 to 13%, respectively, during the first 2 forecast days. Certainly, one must keep in mind that the scores of this study correspond to high-impact weather events that affected a limited geographical area and not to different weather types for long periods (as in the literature). The errors of the near surface parameters are not expected to detrimentally affect the results of this study. Sensitivity analysis was performed by introducing these near surface errors (i.e., overestimation of T2m and mslp, as well as underestimation of Td2m) to the actual radiosonde ascent of Thessaloniki at 00 UTC on 15 July 2014. The outcome was a small lifting of the lifting condensation level (by a few tenths of meters) and a small decrease of the wet bulb potential temperature (<1 K). Thus, the CAPE decreased only by a few percent (~3%) while the CIN remained almost unchanged.

General instability indices from the model simulation were calculated using RIP software. They were calculated for the nearest gridpoint closest to the location of LGTS at 00:00 UTC on 15 July 2014. This was just prior to the onset of the severe convective event, when the observed sounding was available. The predicted values of the instability indices Showalter, LI, K and Total Totals were −1.6, −3.4, 36.0 and 51.0, while their observed values were −1.31, −3.84, 34.1 and 49.8, respectively. The comparison of the model simulated stability indices with the observed ones showed that they were of close magnitude. Similarly, the precipitable water of the actual sounding was 38.73 mm and the simulated one was very close at 39.5 mm. The small difference may be attributed to model errors and to the fact that the humidity was measured up to 300 hPa in the actual sounding, while the model top reached 50 hPa.

At the gridpoints of WRF-D02 which are nearest to the stations of AUTH and LGTS (where the maximum amounts were observed), the model predicted 47.0 mm and 32.7 mm against the observed values of 98.5 mm and 61 mm, respectively. However, 94 mm was simulated about 24 km southeast of AUTH. In an area of about 43 km × 43 km centered at the nearest gridpoint to AUTH, the threshold of 80 mm/24 h was exceeded at 9 gridpoints in the control simulation. Moreover, 56.3 mm (58.2 mm) were predicted about 5.7 km (8.2 km) east (east–southeast) of LGTS. Therefore, it was necessary to evaluate the simulated results of the very high resolution domain (WRF-D02) against the precipitation estimates of the weather radar at Filyro using a neighborhood based approach. Following the methodology of Clark et al. (2010), a hit is considered at a gridpoint when an event is forecast (observed) at the gridpoint and it is observed (forecast) at the same gridpoint or at any grid point within a specified region of this predicted (observed) event. The neighborhood based techniques avoid the "double penalty" problem of the traditional point to point statistical verification of high resolution model forecasts (e.g., Ebert, 2008; Rossa et al., 2008).

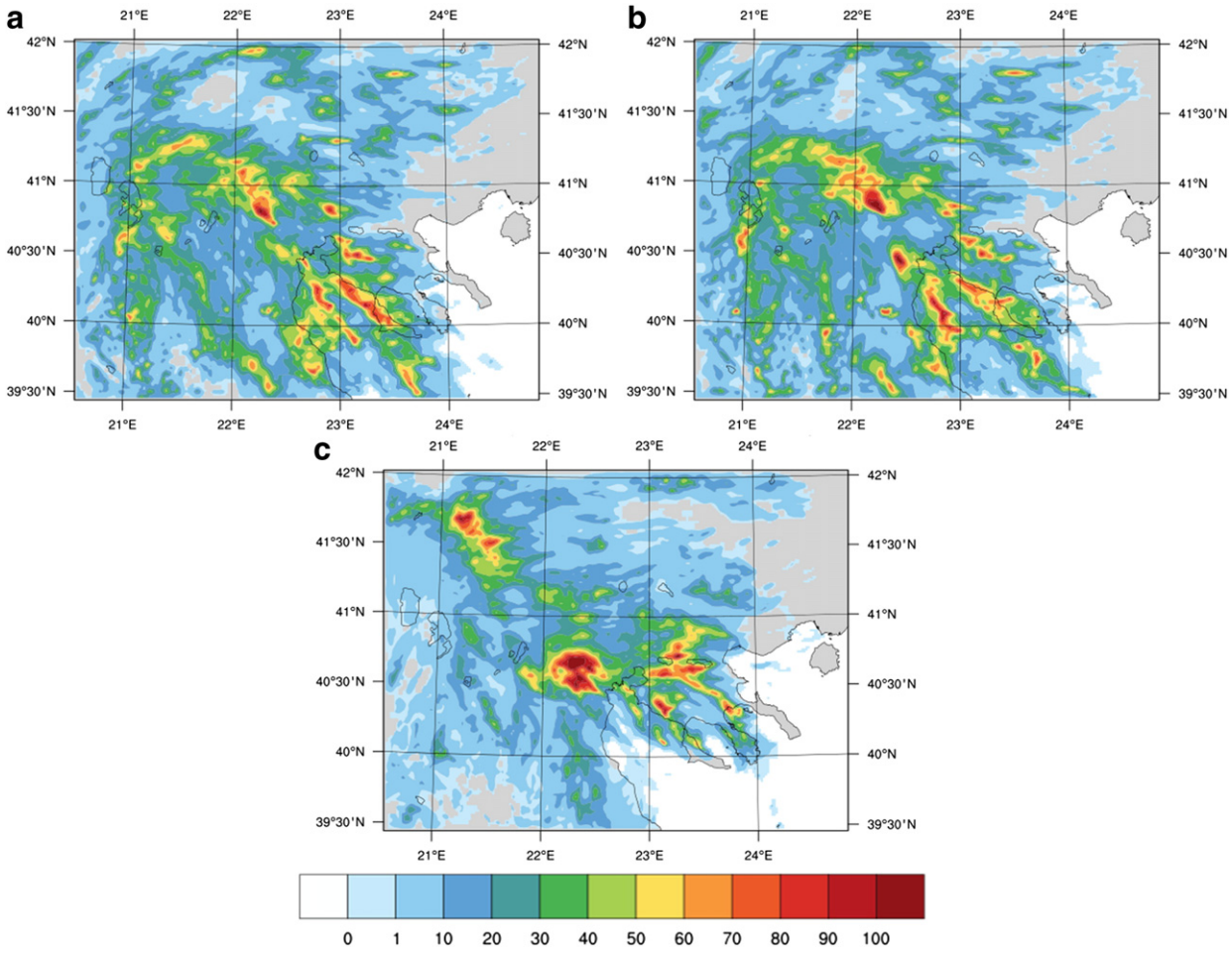

Fig. 12. Total 24-h accumulated precipitation in the three experiments of WRF-D02: a) exp1, b) exp2 and c) exp3. The accumulation was performed from 18:00 UTC on 14 July to 18:00 UTC on 15 July 2014. The color scale indicates the precipitation amount in mm.

Fig. 7 illustrates the categorical neighborhood based scores of the 24 h accumulated precipitation for different neighborhood sizes. The actual size of the specified region is 2Distance × 2Distance (km^2). Therefore, the "Distance" which appears on the x-axis of Fig. 7 represents the half of the side of the square which encompasses each neighborhood region. The confidence intervals were calculated at the 95% significance level using the bootstrapping method (with 1000 subsamples of the matched pairs). The Probability of Detection (POD) of the control simulation (EXP1) exceeded 0.9 at Distances of about 32 km and reached 0.96 at Distances of about 47 km when precipitation events stronger than 60 mm/24 h were considered. The False Alarm Ratio (FAR) dropped to 0.21 at Distances of 50 km. The Equitable Threat Score (ETS) and the Heidke Skill Score (HSS) maximized at about 47 km with values of 0.40 and 0.57, respectively. The maximum values of ETS for different thresholds are illustrated in Fig. 8. At each threshold, the maximum ETS at Distances from 0 to 50 km (i.e., for neighborhood regions up to 100 km × 100 km) is plotted. It appears that the ETS of the control simulation reached 0.71 at the threshold of 35 mm/24 h while it dropped to values below 0.5 at thresholds greater than or equal to 45 mm/24 h (except at 65 mm).

These results are in good agreement with precipitation ETS scores calculated by neighborhood-based verification techniques in Europe (Weusthoff et al., 2010) and the USA (Clark et al., 2010). Weusthoff et al. (2010), who verified COSMO-2 model (with 2.2 km grid spacing) against the Swiss radar data, at the threshold of 5 mm/3 h found ETS scores of 0.14–0.15 at spatial scales of 19.8 and 33 km, which reached 0.17 at 99 km. Clark et al. (2010) verified the NCAR WRF model (at 3 km grid-spacing) which operated over the USA in 2007–08, against NCEP multisensor rainfall estimates. At thresholds of 0.25-in. (6.35 mm) per 3 h they found ETS between about 0.3–0.46 at radii of

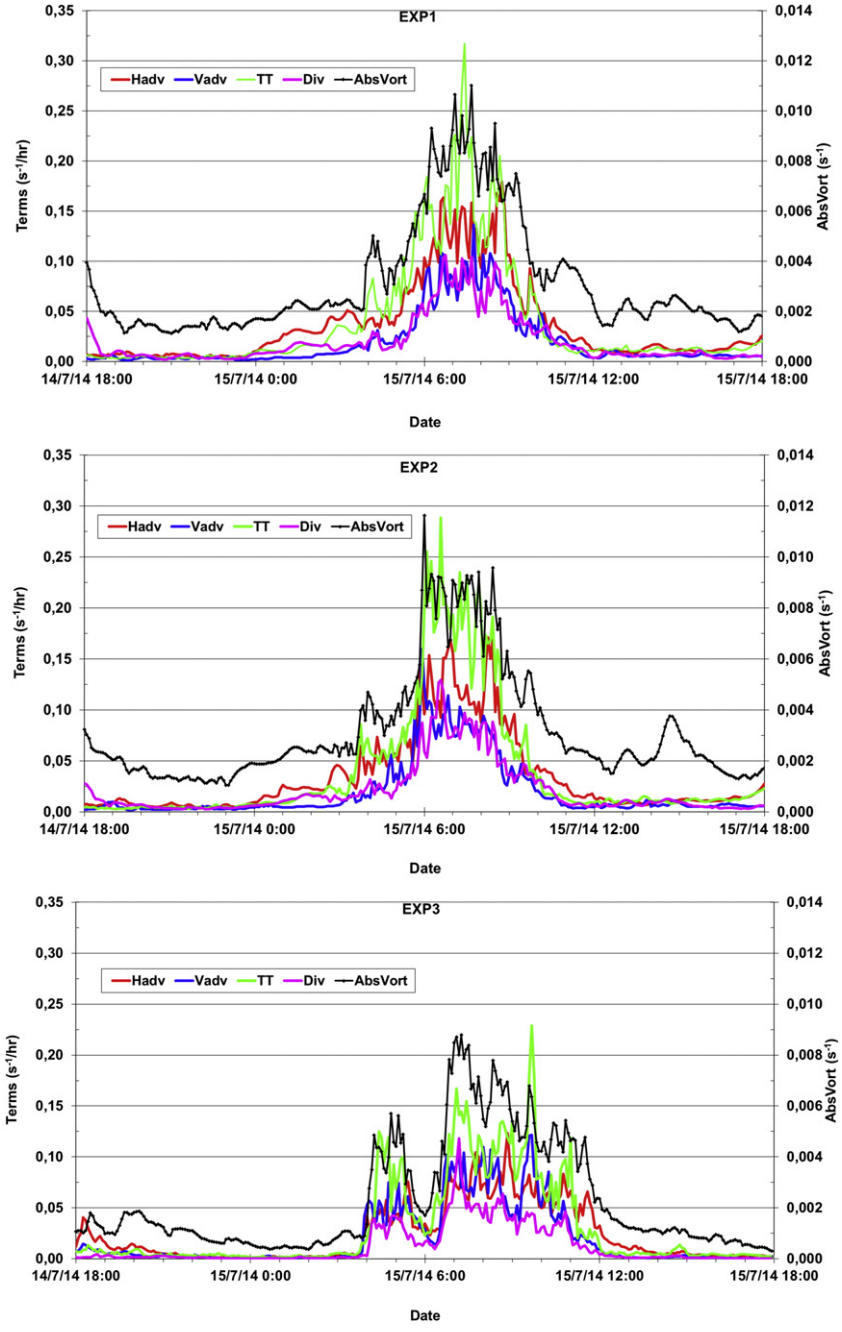

Fig. 13. Timeseries of WRF-D02 maximum simulated values of Absolute Vorticity (s^{-1}) and the vorticity equation terms (s^{-1}/h) of horizontal (Hadv) and vertical advection (Vadv), tilting/twisting (TT) and divergence (Div), at 1 km above sea-level in the area of interest (39.75°N–40.75°N and 22.5°E–24.0°E), for the three experiments.

40–60 km. It is recognized that the accumulation period of the above studies is 3 h compared to 24 h in the present study.

The lightning activity was represented in the simulations through the LPI. Fig. 9 presents the maximum hourly value of LPI, calculated from the 5-min outputs of D02, and the number of lightning detected by Zeus system. Both timeseries were calculated in the area of interest (39.75°N–40.75°N, 22.5°E–24.0°E). The model predicted the occurrence of the activity, but with a delay of about 3 h in its outset and about 1 h in its termination (Fig. 9a). The time of the peak activity was represented with a delay of about 1 h, in good agreement with observations.

The evaluation of the control simulation (exp1) showed that WRF model produced a successful representation of the meteorological conditions during the intense precipitation event of 15 July 2014, despite some discrepancies which were due to the severity of the phenomena. Moreover, its combination with LPI provided a warning of the lightning activity in the area of interest. Therefore, it is concluded that this model setup of the control simulation can be used in the sensitivity experiments.

4.2. Sensitivity experiments

This section investigates the effect of topography on the intense precipitation event of 15 July 2014 and its lightning activity. The area of interest is characterized by large variability in its physiographic characteristics, complex topography and the highest Greek mountain (Mt. Olympus with its highest peak Mytikas rising to 2919 m) at its western side. The second experiment (exp2) employed the SRTM topography in order to examine the effects of this very fine resolution dataset on the modeling of the high impact weather event. In the third experiment (exp3), the model setup was identical to the one of the control simulation (exp1), but the topography was completely removed in the area covered by D02 (in both nests). Smoothing was applied near the boundaries of D01 with D02. The topography of the three rows and columns of D01 which are located just outside D02 was reduced by 25% (3rd row/column far from D02), 50% (2nd one) and 75% (1st one). The aim of this experiment is to understand the importance of topography in this weather event which occurred under strong synoptic forcing.

Fig. 9b indicates that the performance of the second experiment in predicting the potential for lightning activity was more successful than the one of the control experiment, because it reduced the delay of its outset by 1 h and simulated quite well its double peak. On the other hand, the lack of topography in D02 resulted in small but noticeable changes in the time evolution of predicted lightning potential (Fig. 9c). The activity was unrealistically extended by 1 h and multiple peaks appeared. The linear correlation between the hourly time series of the observed lightnings' number and the maximum LPI of the three experiments (24 pairs), was 0.63 (99% significance level; exp1), 0.82 (99% significance level; exp2) and 0.47 (95% significance level; exp3) in the area of interest from 18:00 UTC on 14 July to 18:00 UTC on 15

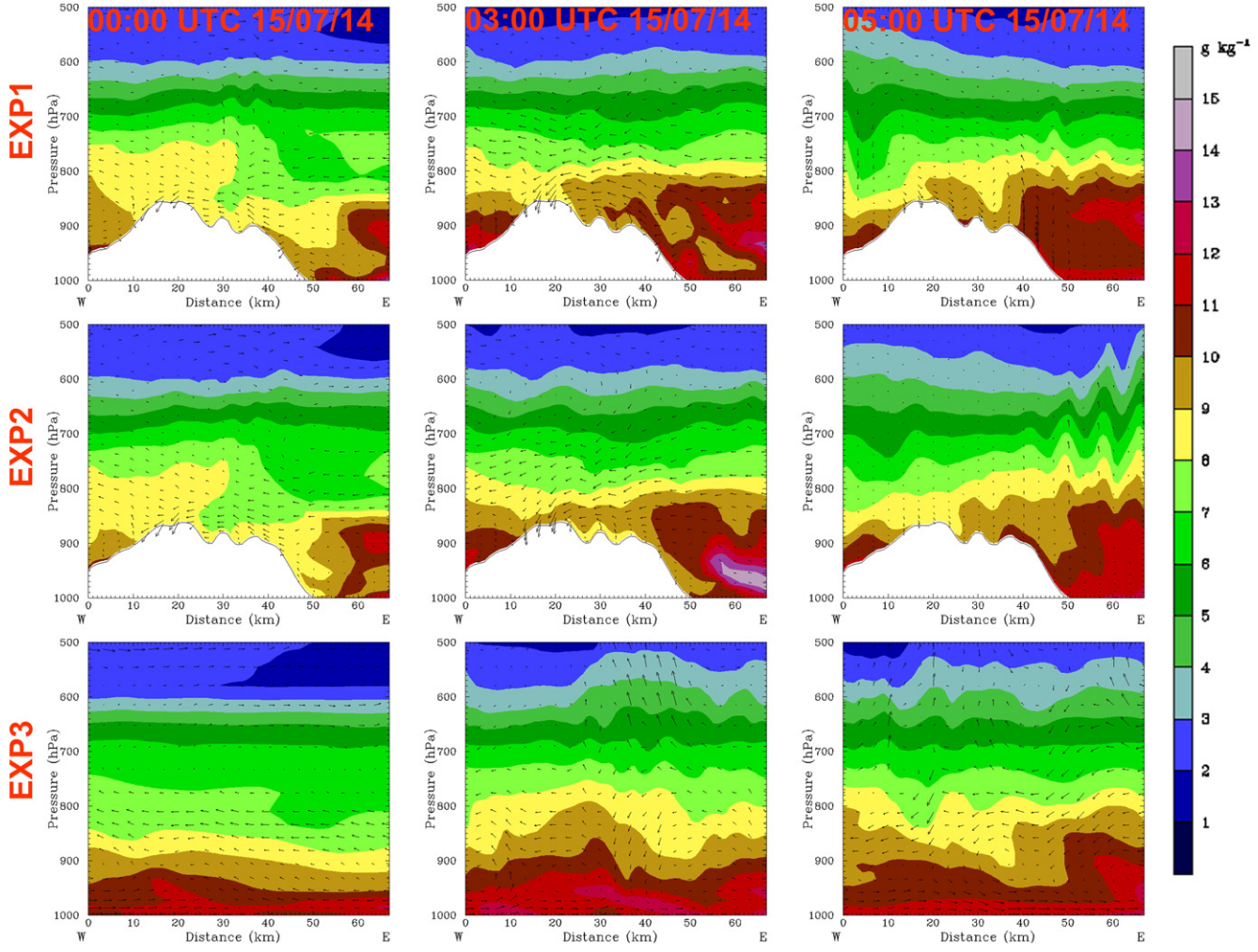

Fig. 14. Vertical sections of WRF-D02 simulated specific humidity (g/kg; shaded) and wind flow along the section (vectors) for the three experiments at 00:00 UTC, 03:00 UTC and 05:00 UTC on 15 July 2014. The edges of the section are 40.15°N, 21.90°E and 40.15°N, 22.70°E. The area of the section is depicted in Fig. 1b. The rows correspond to each experiment, while the columns correspond to each time.

July 2014. The evaluation of the maximum hourly LPI in the area of interest at the same 24 h period is presented in Fig. 10 using categorical statistics. At each hourly interval it was considered to have: a) actual lightning activity if the hourly number of strikes detected by Zeus was greater than zero and b) simulated activity if the hourly maximum of LPI (calculated by the 5 min WRF-D02 output) was non-zero. The highest POD and ETS were exhibited by experiment 2. The 3rd experiment had the same POD as the control run, but higher FAR and lower ETS. Therefore, as far as the time evolution of the simulated lightning activity is concerned, the 2nd experiment appeared to be the most successful, because it predicted its beginning, duration and temporal variability in better agreement with observations.

Sensitivity analysis was performed by omitting LPI values smaller than 10% of the maximum value of LPI at each experiment in the area of interest (39.75°N–40.75°N, 22.5°E–24.0°E), and not in the entire high resolution domain (D02). This means that the LPI values of 3.9 J/kg (at 10 UTC 15 July 2014 in experiment 1; Fig. 9a) and 5.8 J/kg (at 10 UTC 15 July 2014 in experiment 2; Fig. 9b) were not considered to correspond to simulated activity. This led to: i) a reduction of FAR of experiments 1 and 2 to zero and ii) an increase of ETS of experiments 1 and 2 to 0.56 and 0.69, respectively. Therefore, the conclusions about the performance of each experiment to simulate the time evolution of lightning activity did not change and the best scores were still exhibited by experiment 2 followed by experiment 1. However, in this case the importance of orography on the simulation of lightning activity became more evident.

The spatial variability and extent of the LPI in the entire D02, averaged from 18:00 UTC on 14 July to 18:00 UTC on 15 July 2014, is illustrated in Fig. 11. The lack of values near the boundaries is due to the methodology used for the calculation of the index. At each grid-point, LPI may take non-zero values only within the "charging zone" (0 °C to −20 °C) of the thunderstorm, when the majority of the model grid-points in a radius of 10 km has vertical velocity greater than 0.5 m/s (Yair et al., 2010). Therefore, the index was calculated only at the grid points which were located at least 10 km far from the boundaries of D02. The spatial extent of the predicted activity is very similar in experiments 1 and 2, and is in good agreement with the observations (Fig. 11d). Both experiments indicated the threat at the areas of Thermaikos Gulf, Chalkidiki and Thessaloniki. The various inaccuracies/misplacements of the simulated lightning threat may be due to model errors, initialization errors and to the complexity of atmospheric processes involved in the calculation of LPI. The 3rd experiment suggests that although this weather event occurred under strong synoptic forcing, the lack of topography resulted in a significant misplacement of the highest LPI values over the land west of Thessaloniki where no actual strikes were detected. Certainly, this experiment also represented the threat over the regions of Chalkidiki and Thessaloniki.

The influence of the topography changes on the total precipitation accumulated from 18:00 UTC on 14 July to 18:00 UTC on 15 July 2014, is depicted in Fig. 12. The two experiments with the actual topography predicted high precipitation amounts not only in Thessaloniki and Chalkidiki, but also in the Thermaikos Gulf where the lightning observations indicated the occurrence of convective activity. On the other hand, in the experiment without topography (experiment 3) strong precipitation was simulated in Thessaloniki and Chalkidiki, but not in Thermaikos Gulf since extremely large amounts (up to 128 mm/24 h locally) were unrealistically predicted west of Thessaloniki. Finally, it is noted that all experiments predicted intense precipitation (>60 mm/24 h) close to Thessaloniki where the floods occurred. In an area of about

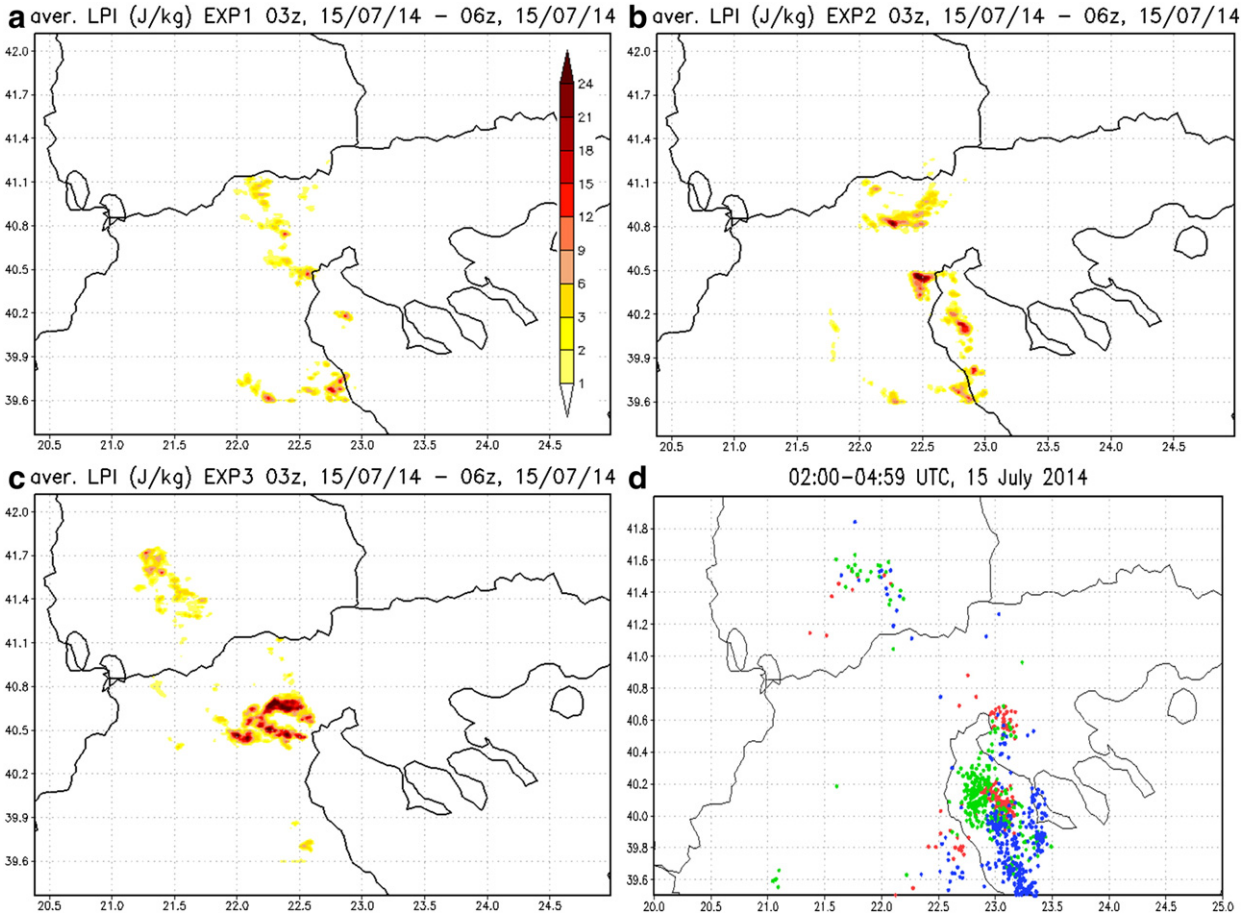

Fig. 15. a, b, c) The average value of LPI (J/kg) in the three experiments from 03:00 UTC to 06:00 UTC on 15 July 2014, and d) the locations of lightning strikes detected by Zeus system from 02:00 UTC to 04:59 UTC on 15 July 2014. In panel (d), red color: 02:00–02:59 UTC, green color: 03:00–03:59 UTC and blue color: 04:00–04:59 UTC. The color scale indicates the average LPI in J/kg.

30 km × 30 km (361 gridpoints) centered at the nearest gridpoint to AUTH, where the maximum precipitation was recorded, the threshold of 60 mm was exceeded at 23 (6.4%), 19 (5.3%) and 22 (6.1%) gridpoints in experiments 1 to 3, respectively. In agreement with these results, Fig. 7 shows that the 3rd experiment exhibited the lowest maximum scores of POD, ETS, HSS and the highest minimum False Alarm Ratio (which were statistically significant at the 95% level) at Distances up to 50 km. Similarly, experiment 3 had had systematically the lowest scores of maximum ETS at all thresholds (Fig. 8). Figs. 7 and 8 also show that the 2nd experiment produced the best forecasts of precipitation at high thresholds (greater than 50 mm/24 h).

The absolute vorticity budget was used in order to study the influence of topography on the dynamical processes that affected the precipitation and lightning event, following the methodology of Matsangouras et al. (2014). This is a useful tool which is commonly applied in studies of atmospheric dynamics. The absolute vorticity and the vorticity equation terms were derived at 5 min intervals at a height of 1 km above sea-level. This height was selected because it is generally located near the base of thunderstorms and in the simulations it was generally found above the model topography in the area of interest (except from its SW corner and a few gridpoints in Chalkidiki). The calculations were based on the WRF-D02 simulations. The necessary upper air fields were vertically interpolated at 250 m intervals before the calculation of the vertical derivatives. The derivatives were estimated by second order centered finite differences. The grid-points with topography above or equal to 750 m (which was the lower level in the vertical derivatives) were not considered.

Fig. 13 illustrates timeseries of the maximum values of the absolute vorticity and of the vorticity equation terms of horizontal and vertical advection, tilting/twisting and divergence in the area of interest (39.75°N–40.75°N, 22.5°E–24.0°E). The solenoidal term was at least four orders of magnitude smaller than the other terms and it was not plotted. The simulations with topography were associated with higher values of maximum absolute vorticity in the area of interest than the experiment without topography (Fig. 13). The maximum absolute vorticity was about 0.012 s^{-1} and appeared in the 2nd experiment (with the high resolution topography). The most important term of the vorticity equation appeared to be the twisting/tilting of horizontal vorticity to the vertical direction, with values up to 0.32 s^{-1}/h, 0.29 s^{-1}/h and 0.23 s^{-1}/h in experiments 1, 2 and 3, respectively. The predominance of this term was probably associated with the strong vertical shear of the horizontal wind which reached area-averaged (39.75°N–40.75°N, 22.5°E–24.0°E) magnitudes of 8.3 m/s and 6 m/s for its u and v components, respectively, between 700 and 950 hPa in the control experiment (not shown). The vertical shear is also an important factor for long-lived convective storms. The lack of topography in the 3rd experiment may have also contributed to the occurrence of weaker horizontal gradients of the vertical wind component. The second most important term was generally the horizontal advection of vorticity due to the approaching mid-tropospheric closed low. The vertical advection and the divergence terms were generally equally important to each other and less important than the twisting/tilting and the horizontal advection terms (mainly in experiments 1 and 2). At higher altitudes (not shown) the horizontal and vertical advection terms increased and became equally important to the twisting/tilting term. In the mid-troposphere the vertical advection term was the dominant one (not shown). Regarding the time evolution of the maximum absolute vorticity at 1 km height (Fig. 13), its increase occurred between 03 and 05 UTC in good agreement with the triggering of lightning activity in the 3 simulations (Fig. 9). Actually, the maximum vorticity increased firstly in the 2nd experiment in the area of interest, similarly to what happened in the simulated lightning activity.

Fig. 14 displays zonal sections of specific humidity and wind flow (u and omega) across the mountain range located at the western boundary of the area of interest (40.15°N, 21.90°E–40.15°N, 22.70°E) from the three experiments. The results are shown at 00:00, 03:00 and 05:00 UTC on 15 July 2014, before and just after the onset of simulated lightning activity (Fig. 9). Air masses with high values of moisture (>10 g/kg) were advected from the Gulf of Thermaikos to the land regions under the influence of the low-level easterly current. In the two experiments with topography, the air masses were lifted on the eastern side of the mountains triggering convection. Fig. 12 shows that in experiments 1 and 2, larger precipitation amounts were simulated east of these mountains in the Gulf of Thermaikos and along its western coastline. It needs to be noted that moist air masses also crossed the orography to promote precipitation farther west (Fig. 12a, b) outside the area of interest, west of 22°E. The lack of topography in the 3rd experiment allowed the moist air masses to penetrate over the land, without being lifted on the western coastline of the Gulf of Thermaikos. In this case, the precipitation amounts in the Gulf were much smaller than in the experiments with topography and the areas of convective activity appeared mainly over land (Figs. 11, 12) and were determined by the synoptic forcing of the upper tropospheric flow and local convergence zones.

During the first hours of the event (03:00–06:00 UTC in the experiments vs 02:00–05:00 UTC in Zeus data) a comparison of the simulated with the actual lightning activity is also presented in Fig. 15. The first lightning strikes were observed on the eastern side of the north–south oriented mountain range west of the Gulf of Thermaikos (Pieria mountains and Olympos), in the Gulf of Thermaikos and in the vicinity of Thessaloniki. The two experiments with topography exhibited a similar pattern of the 3 h averaged LPI, predicting lightning activity in the Gulf and along its western coast (probably in thunderstorms that were due to orographic lifting). However, the 2nd one predicted higher values of LPI and mainly provided a more pronounced indication of the lightning threat in Thermaikos in better agreement with observations (Fig. 15d). On the contrary, the lack of topography in experiment 3 resulted in no simulated lightning in the Gulf. Finally, all the experiments did not manage to provide indication of the lightning threat in Thessaloniki during the onset of the event of this study.

5. Summary — conclusions

An intense precipitation event associated with lightning activity affected Thessaloniki, Chalkidiki and Thermaikos Gulf on 15 July 2014. The station of AUTH, which is located near the center of Thessaloniki, measured 98.5 mm of rain in 15 h. Also, the station of the airport of Thessaloniki recorded 61 mm of rain in 12 h. The maximum rate at AUTH reached 41 mm/3 h in each one of the periods 00:00–03:00 UTC and 06:00–09:00 UTC on 15 July 2014. The measurement of AUTH is a record maximum for all seasons. The instability indices and the high values of CAPE indicated that the event took place in an environment that could support thunderstorm activity. The development of this intense event was associated with significant low-level convergence and upper-level divergence even before its triggering and relative vorticity advection, since the area of interest was located ahead of an approaching mid-tropospheric closed low.

The high resolution (1.667 km × 1.667 km) non-hydrostatic WRF-ARW numerical weather prediction model simulated this intense precipitation event, while the Lightning Potential Index was calculated from WRF model output. This index estimated the potential for lightning activity. The model results were in good agreement with the available observations of mean sea-level pressure, temperature, humidity and the instability indices of the sounding at Thessaloniki's airport. The application of neighborhood-based statistical verification against radar data showed that the model simulated the occurrence of intense precipitation in the vicinity of Thessaloniki. The sensitivity experiments suggested that the precipitation and lightning event of this study was affected by topography. Strong precipitation and intense lightning were predicted even in the 3rd experiment, associated with convection that developed during the period of strong synoptic forcing. Nevertheless, topographical variations in elevation also had a strong influence

on the spatial distribution and intensity of each. The application of the very fine resolution topography of NASA Shuttle Radar Topographic Mission improved the simulated precipitation and the calculated lightning potential. However, further investigation is needed in order to clarify its role on small scale circulations and their non-linear interactions. Additional studies would be useful to help forecasters understand the potential model limitations in predicting intense precipitation and lightning activity, and the potential utility of using the neighborhood approach to warn about possible severe conditions within certain sensitive areas.

Acknowledgments

The observed lightning data were provided by the ground-based ZEUS network operated by the National Observatory of Athens. ZEUS is a very low frequency (VLF) based lightning detection system. Detailed presentation of the system is given in Kotroni and Lagouvardos (2008) and Lagouvardos et al. (2009). We would also like to thank the Hellenic National Meteorological Service, the National Observatory of Athens and the ECMWF for making available the surface observations and gridded analyses, the private company 3D S.A. for providing the weather radar data, the University of Wyoming for the radiosonde data, NCAR for the WRF numerical model as well as Max-Planck-Institut for the CDO software. The Model Evaluation Tools (MET) was developed at the National Center for Atmospheric Research (NCAR) through a grant from the United States Air Force Weather Agency (AFWA). NCAR is sponsored by the United States National Science Foundation. Finally, we would like to thank the two anonymous reviewers for their careful and constructive review that allowed for the improvement of our article.

References

Anagnostopoulou, C., Tolika, K., 2012. Extreme precipitation in Europe: statistical threshold selection based on climatological criteria. Theor. Appl. Climatol. 107, 479–489. http://dx.doi.org/10.1007/s00704-011-0487-8.

Ashley, W.S., Gilson, C.W., 2009. A reassessment of U.S. lightning mortality. Bull. Am. Meteorol. Soc. 90, 1501–1518.

Bartzokas, A., Kotroni, V., Lagouvardos, K., Lolis, C.J., Gkikas, A., Tsirogianni, M.I., 2010. Weather forecast in north-western Greece: RISKMED warnings and verification of MM5 model. Nat. Hazards Earth Syst. Sci. 10, 383–394.

Bright, D.R., Wandishin, M.S., Jewell, R.E., Weiss, S.J., 2005. A physically based parameter for lightning prediction and its calibration in ensemble forecasts. Conference on Meteorological Applications of Lightning Data. Am. Meteorol. Soc, San Diego, Calif., U.S.A.

Chen, F., Dudhia, J., 2001. Coupling an advanced land-surface/hydrology model with the Penn State/NCAR MM5 modeling system. Part I: model description and implementation. Mon. Weather Rev. 129, 569–585.

Clark, A.J., Gallus Jr., W.A., Weisman, M.L., 2010. Neighborhood-based verification of precipitation forecasts from convection-allowing NCAR WRF model simulations and the operational NAM. Weather Forecast. 25, 1495–1509. http://dx.doi.org/10.1175/2010WAF2222404.1.

Dahl, J.M.L., Höller, H., Schumann, U., 2011a. Modeling the flash rate of thunderstorms. Part I: framework. Mon. Weather Rev. 139, 3093–3111.

Dahl, J.M.L., Höller, H., Schumann, U., 2011b. Modeling the flash rate of thunderstorms. Part II: implementation. Mon. Weather Rev. 139, 3112–3124.

Defer, E., Lagouvardos, K., Kotroni, V., 2005. Lightning activity in the eastern Mediterranean region. J. Geophys. Res. 110, D24210. http://dx.doi.org/10.1029/2004JD005710.

Ebert, E.E., 2008. Fuzzy verification of high resolution gridded forecasts: a review and proposed framework. Meteorol. Appl. 15, 51–64.

Efstathiou, G.A., Zoumakis, N.M., Melas, D., Lolis, C.J., Kassomenos, P., 2013. Sensitivity of WRF to boundary layer parameterizations in simulating a heavy rainfall event using different microphysical schemes. Effect on large-scale processes. Atmos. Res. 132–133, 125–143. http://dx.doi.org/10.1016/j.atmosres.2013.05.004.

Fierro, A.O., Mansell, E.R., Ziegler, C.L., MacGorman, D.R., 2012. Application of a lightning data assimilation technique in the WRF-ARW model at cloud-resolving scales for the tornado outbreak of 24 May 2011. Mon. Weather Rev. 140, 2609–2627. http://dx.doi.org/10.1175/MWR-D-11-00299.1.

Giannaros, T.M., Kotroni, V., Lagouvardos, K., 2015. Predicting lightning activity in Greece with the Weather Research and Forecasting (WRF) model. Atmos. Res. 156, 1–13.

Holton, J.R., 1992. An Introduction to Dynamic Meteorology. 3rd edition. Academic Press, p. 511.

Hong, S.-Y., Lim, J.-O.J., 2006. The WRF Single-Moment 6-Class Microphysics Scheme (WSM6). J. Korean Meteorol. Soc. 42, 129–151.

Hong, S.-Y., Pan, H.-L., 1996. Nonlocal boundary layer vertical diffusion in a medium-range forecast model. Mon. Weather Rev. 124, 2322–2339.

Hong, S.-Y., Noh, Y., Dudhia, J., 2006. A new vertical diffusion package with an explicit treatment of entrainment processes. Mon. Weather Rev. 134, 2318–2341.

Hoskins, B.J., McIntyre, M.E., Robertson, A.W., 1985. On the use and significance of isentropic potential vorticity maps. Q. J. R. Meteorol. Soc. 111, 877–946.

Iacono, M.J., Delamere, J.S., Mlawer, E.J., Shephard, M.W., Clough, S.A., Collins, W.D., 2008. Radiative forcing by long-lived greenhouse gases: calculations with the AER radiative transfer models. J. Geophys. Res. 113, D13103. http://dx.doi.org/10.1029/2008JD009944.

Kain, J.S., 2004. The Kain–Fritsch convective parameterization: an update. J. Appl. Meteorol. 43, 170–181.

Kallos, G., Pytharoulis, I., 2005. Short-term predictions (weather forecasting purposes). In: Anderson, M.G. (Ed.), Encyclopedia of Hydrological Sciences. Wiley, London, pp. 2791–2811.

Karacostas, T.S., 1984. The design of the Greek national hail suppression program. Ninth Conference on Weather Modification. American Meteorological Society, Park City, Utah, U.S.A.

Katsanos, D., Kotroni, V., Lagouvardos, K., 2009. Lightning in the Mediterranean in relation with cloud microphysical parameters. In: Betz, H.D., et al. (Eds.), Lightning: Principles, Instruments and Applications. Springer Science, pp. 433–446.

Kornaros, G., 1999. Tables of Climatological Data of the Greek Stations. Department of Climatology and Applications. Hellenic National Meteorological Service, p. 128 (in Greek).

Kotroni, V., Lagouvardos, K., 2008. Lightning occurrence in relation with elevation, terrain slope and vegetation cover in the Mediterranean. J. Geophys. Res. 113, D21118.

Kotroni, V., Kallos, G., Lagouvardos, K., 1997. Convergence zones over the Greek Peninsula and associated thunderstorm activity. Q. J. R. Meteorol. Soc. 123, 1961–1984.

Kotroni, V., Lagouvardos, K., Kallos, G., Ziakopoulos, D., 1999. Severe flooding over central and southern Greece associated with pre-cold frontal orographic lifting. Q. J. R. Meteorol. Soc. 125, 967–991.

Lagouvardos, K., Kotroni, V., Dobricic, S., Nickovic, S., Kallos, G., 1996. The storm of October 21–22 1994 over Greece: observations and model results. J. Geophys. Res. 101D, 26217–26226.

Lagouvardos, K., Kotroni, V., Betz, H.-D., Schmidt, K., 2009. A comparison of lightning data provided by ZEUS and LINET networks over Western Europe. Nat. Hazards Earth Syst. Sci. 9, 1713–1717.

Lynn, B.H., Yair, Y., Price, C., Kelman, G., Clark, A.J., 2012. Predicting cloud-to-ground and intracloud lightning in weather forecast models. Weather Forecast. 27, 1470–1488. http://dx.doi.org/10.1175/WAF-D-11-00144.1.

Lynn, B.H., Kelman, G., Ellrod, G., 2015. An evaluation of the efficacy of using observed lightning to improve convective lightning forecasts. Weather Forecast. 30, 405–423. http://dx.doi.org/10.1175/WAF-D-13-00028.1.

Mass, C., Ovens, D., Westrick, K., Colle, B., 2002. Does increasing horizontal resolution produce more skilful forecasts? Bull. Am. Meteorol. Soc. 83, 407–430.

Matsangouras, I.T., Pytharoulis, I., Nastos, P.T., 2014. Numerical modeling and analysis of the effect of complex Greek topography on tornadogenesis. Nat. Hazards Earth Syst. Sci. 14, 1905–1919. http://dx.doi.org/10.5194/nhess-14-1905-2014.

Mazany, R.A., Businger, S., Gutman, S.I., Roeder, W., 2002. A lightning prediction index that utilizes GPS integrated precipitable water vapour. Weather Forecast. 17, 1034–1047.

Mazarakis, N., Kotroni, V., Lagouvardos, K., Argiriou, A., 2008. Storms and lightning activity in Greece during the warm period of 2003–06. J. Appl. Meteorol. 47, 3089–3098.

Mazarakis, N., Kotroni, V., Lagouvardos, K., Argiriou, A.A., 2009. The sensitivity of numerical forecasts to convective parameterization during the warm period and the use of lightning data as an indicator for convective occurrence. Atmos. Res. 94, 704–714. http://dx.doi.org/10.1016/j.atmosres.2009.03.002.

McGaul, E.W., Goodman, S.J., LaCasse, K.M., Cecil, D.J., 2009. Forecasting lightning threat using cloud-resolving model simulations. Weather Forecast. 24, 709–729.

Nastos, P.T., Matsangouras, I.T., Chronis, T.G., 2014. Spatio-temporal analysis of lightning activity over Greece — preliminary results derived from the recent state precision lightning network. Atmos. Res. 144, 207–217.

Nie, Z., Zhao, W., Zhang, P., Wen, Y., Chen, W., 2008. Power network lightning accident quick inquiry with the lightning location system. Geo-Spat. Inf. Sci. 11, 43–48.

Papadopoulos, A., 2001. A Regional Numerical Model with Special Capabilities in the Use of the Initial and Boundary Conditions (Ph.D. Thesis), School of Physics, University of Athens, Athens, p. 272 (in Greek).

Papadopoulos, A., Katsafados, P., 2009. Verification of operational weather forecasts from the POSEIDON system across the Eastern Mediterranean. Nat. Hazards Earth Syst. Sci. 9, 1299–1306. http://dx.doi.org/10.5194/nhess-9-1299-2009.

Papadopoulos, A., Chronis, T.G., Anagnostou, E.N., 2005. Improving convective precipitation forecasting through assimilation of regional lightning measurements in a meso-scale model. Mon. Weather Rev. 133, 1961–1977.

Papadopoulos, A., Serpetzoglou, E., Anagnostou, E.N., 2009. Evaluating the impact of lightning data assimilation on mesoscale model simulations of a flash flood inducing storm. Atmos. Res. 94, 715–725.

Papagiannaki, K., Lagouvardos, K., Kotroni, V., 2013. A database of high-impact weather events in Greece: a descriptive impact analysis for the period 2001–2011. Nat. Hazards Earth Syst. Sci. 13, 727–736.

Peterson, D., Wang, J., Ichoku, C., Remer, L.A., 2010. Effects of lightning and other meteorological factors on fire activity in the north American boreal forest: implications for fire weather forecasting. Atmos. Chem. Phys. 10, 6873–6888.

Price, C., Rind, D., 1992. A simple lightning parameterization for calculating global lightning distributions. J. Geophys. Res. 97 (D9), 9919–9933.

Pytharoulis, I., Feidas, H., Karakostas, T., 2012. Study of lightning activity with the use of high resolution simulations. Geographies 20, 51–78 (in Greek with English abstract).

Pytharoulis, I., Tegoulias, I., Kotsopoulos, S., Bampzelis, D., Karacostas, Th., Katragkou, E., 2014. Evaluation of the operational numerical weather predictions of the WaveForUs

project. 12th International Conference of Meteorology, Climatology and Physics of the Atmosphere, Heraklion, Greece, 28–31 May 2014. vol. 3, pp. 96–101.
Rakov, V.A., Uman, M.A., 2003. Lightning: Physics and Effects. Cambridge University Press.
Renni, E., Krausmann, E., Cozzani, V., 2010. Industrial accidents triggered by lightning. J. Hazard. Mater. 184, 42–48.
Rossa, A., Nurmi, P., Ebert, E., 2008. Overview of methods for the verification of quantitative precipitation forecasts. In: Michaelides, S. (Ed.), Precipitation: Advances in Measurement, Estimation and Prediction, pp. 417–450.
Sindosi, O.A., Bartzokas, A., Kotroni, V., Lagouvardos, K., 2015. Influence of orography on precipitation amount and distribution in NW Greece; a case study. Atmos. Res. 152, 105–122. http://dx.doi.org/10.1016/j.atmosres.2014.06.013.
Sioutas, M., Rudolph, R.C., 1993. Z–R relationships for summertime convective rainfall in northern Greece. 4th International Conference on Precipitation, Sponsored by NASA, NOAA, The University of Iowa and AGU, AMS, Iowa City, April 26–28.
Skamarock, W.C., Klemp, J.B., Dudhia, J., Gill, D.O., Barker, D.M., Duda, M.G., Huang, X.Y., Wang, W., Powers, J.G., 2008. A description of the advanced research WRF version 3. NCAR/TN-475+STRp. 113.
Wang, W., Bruyère, C., Duda, M., Dudhia, J., Gill, D., Kavulich, M., Keene, K., Lin, H.-C., Michalakes, J., Rizvi, S., Zhang, X., Beezley, J., Coen, J., Mandel, J., Chuang, H.-Y., McKee, N., Slovacek, T., Wolff, J., 2013. ARW Version 3 Modeling System User's Guide. NCAR-MMM 411.
Weusthoff, T., Ament, F., Arpagaus, M., Rotach, M.W., 2010. Assessing the benefits of convection-permitting models by neighborhood verification: examples from MAP D-Phase. Mon. Weather Rev. 138, 3418–3433.
Yair, Y., Lynn, B., Price, C., Kotroni, V., Lagouvardos, K., Morin, E., Mugnai, A., Llasat, M.d.C., 2010. Predicting the potential for lightning activity in Mediterranean storms based on the WRF model dynamic and microphysical fields. J. Geophys. Res. 115, D04205.